UCRL-CONF-203613

LAWRENCE LIVERMORE NATIONAL LABORATORY

Reconstruction of quasi-monochromatic images from a multiple monochromatic x-ray imaging diagnostic for inertial confinement fusion

N. Izumi, R.E. Turner, T.W. Barbee, J.A. Koch, L.A. Welser, R.C. Mansini

April 16, 2004

15th Topical Conference on High Temperature Plasma Diagnostics
San Diego, CA, United States
April 19, 2004 through April 22, 2004

Reconstruction of quasi-monochromatic images from a multiple monochromatic x-ray imaging diagnostic for inertial confinement fusion experiment

N. Izumi, R. E. Turner, T. W. Barbee, J. A. Koch

University of California, Lawrence Livermore National Laboratory, Livermore CA, USA

L. A. Welser, R. C. Mancini

Department of Physics, university of Nevada/Reno, Reno NV, USA

We have developed a software package for image reconstruction of a multiple monochromatic x-ray imaging diagnostics (MMI) for diagnostic of inertial conferment fusion capsules. The MMI consists of a pinhole array, a multi-layer Bragg mirror, and a charge injection device image detector (CID). The pinhole array projects ~500 sub-images onto the CID after reflection off the multi-layer Bragg mirror. The obtained raw images have continuum spectral dispersion on its vertical axis. For systematic analysis, a computer-aided reconstruction of the quasi-monochromatic image is essential.

I. INTRODUCTION

In inertial confinement fusion experiments, X-ray line emissions from Ar dopant have been utilized for diagnostic of electron temperature, electron number density of compressed core region[1]. With measuring x-ray transmission though high-Z doped layer, one can measure the areal density ($\Delta\rho R$) of ablator region[2]. To obtain spatial information of these physical conditions, quasi-monochromatic imaging of the x-ray emission is crucial. Technically, two different methods of the quasi-monochromatic X-ray imaging have been developed. One approach is imaging with bent-Bragg mirrors[3]. Another approach is imaging with a pinhole array coupled with a flat Bragg mirror[4]. An advantage of the pinhole-Bragg mirror couple is flexible post process capability with a reconstruction program. Because the raw image covers wide spectral range (i.e. 3~6 keV), one can reconstruct various quasi-monochromatic images of different spectral region (Ar-Ly-α, Ar-Ly-β, Ar-He-α, Ar-He-β, and continuum emission of a vicinity of the line emissions) from a raw image. Due to continuous spectral dispersion of the Bragg mirror, the spectral bandwidth of reconstruction can be chosen arbitrary. In virtue of this flexible reconstruction capability, one can select appropriate bandwidth for each spectral range and subtract background component due to continuum emission and/or satellite emissions.

II. EXPERIMENTAL SETUP

Figure 1 shows experimental set up of the multiple monochromatic imaging (MMI). A pinhole plate (an array of 1280 5-μm-diameter pinholes in 25-μm-thick Ta substrate) was placed 16 mm from the indirect driven target of OMEGA laser facility[5]. Then images are reflected by a WB_4C Bragg mirror (inter planar spacing: 1.51nm, placed 82mm from the target). Rays only which satisfies Bragg condition are projected onto a charge injection device[6] (CID) placed 143 mm from the target. The estimated spatial resolution of the system is ~10 μm on the object plane. Figure 2 shows a typical raw image obtained in indirect drive target. About 500 sub-images are projected on to CID. Vertical position of raw image has approximately linear correspondence to the wavelength.

III. RECONSTRUCTION PRECEDURE

For systematic analysis of quasi-monochromatic image, development of systematic image reconstruction software is crucial[7]. The software can perform background subtraction, spectrum extraction, calibration of spectral sensitivity, estimation of each pinhole position, and reconstruction of quasi-monochromatic image.

a. Extract spectral feature

After subtracting CID's static background from the raw image, we transform the raw image h(x,y) to spatial frequency space $H(n_x,n_y)$ by using 2-dimensinal fast-Fourier-transform (FFT).

$$H(n_x,n_y)=\sum_{k_x=0}^{N_x-1}\sum_{k_y=0}^{N_y-1}\exp(2\pi i k_y n_y/N_y)\exp(2\pi i k_x n_x/N_x)h\left(k_y,k_x\right) \quad (1)$$

Where N_x, N_y are the horizontal and vertical size of the raw image, n_x,n_y and k_x,k_y are pixel position in the raw and FFT image. Figure 3 shows the FFT image of figure 2.

One can extract a horizontally-integrated vertical image profile $f(k_y)$ of the row image by the inverse Fourier transform as,

$$f(k_y) = \frac{1}{N_y} \sum_{k_y=0}^{N_y-1} \exp(-2\pi i k_y n_y / N_y) H\left(k_y, 0\right) \tag{2}$$

Obtained vertical profile has peaks and dips corresponding to emission lines and absorption lines. By identifying each peak in the profile, one can calibrate the spectral dispersion of the system. Spectral sensitivity of the system was calculated from the transmission of filters[8], the reflectivity of the Bragg mirror[9], and the sensitivity of the CID[6].

b. Estimate origins of sub images

The reconstruction process is to sum up many fragments of sub-images obtained by different pinholes,

$$I(x',y') = \frac{\sum_{j=0}^{N_S(x',y')} h(x'-x_j, y'-y_j)}{N_S}, \tag{3}$$

where (x’,y’) is coordinate of the reconstructed image, (x_j,y_j) gives center of j-th sub image in the raw image, Ns(x’.y’) is number of sub images contributing the reconstruction of I(x’.y’). In order to integrate all fragments in right position, precise estimation of sub image center (x_j,y_j) is crucial. However, when we use target mounted pinhole array, the position and orientation of the pinhole array vary shot by shot. Thus we estimated each pinhole position by assuming symmetry of the raw image. Assuming all pinholes are linearly aligned and each sub-image has similar profile, we can estimate the arrangement of the array with numerical fitting. We modeled pinhole function with six parameters; origin of the sub image (x_0,y_0), horizontal and vertical interval of sub images (Dx, Dy), orientation of rows and columns of the sub image array (θ,ϕ). A sub-routine generates simulated image using these parameters,

$$
\begin{aligned}
&g(k_x,k_y) = A(1+\cos\omega_x)^2(1+\cos\omega_y)^2 \\
&where \\
&\begin{pmatrix}\omega_x\\ \omega_y\end{pmatrix} \equiv 2\pi\begin{pmatrix}\cos\theta & \sin\theta\\ \cos\phi & \sin\phi\end{pmatrix}\begin{pmatrix}(k_x-x_0)/D_x\\ (k_y-y_0)/D_y\end{pmatrix},
\end{aligned} \tag{4}
$$

and A is an arbitrary constant.

Then likelihood of the simulated image and the raw data was evaluated by calculating correlation of h and g as,

$$C = \sum_{n_x}\sum_{n_y} H(n_x,n_y)G^*(n_x,n_y) \tag{5}$$

were G is a FFT of simulated image.

The six parameters were optimized to have maximum correlation. We utilized Powell's method for iterative optimization method of parameters. Since the initial values of fitting parameters are inferred from distinct first order peaks of H, the Powell's method[9] converges to unique optimal point without trapped by other local minimums.

By using this optimized parameter set, the reconstruction program calculate the pinhole function (x_j,y_j) and the number of the sub images in given spectral range. Then quasi-monochromatic images were reconstructed as described by equation (3).

IV. CONCLUSION

Figure 4 shows various quasi-monochromatic images reconstructed from figure2. One can reconstruct line image with flexible spectral ranges. While analyzing line emission images, overlapped continuum emission due to Bremsstrahlung can be a background. In order to subtract this background from line emission, we have to obtain image of continuum emission also. With this program, one can easily obtain this continuum image by reconstructing a spectral region next to the line emission. Since the same instruments obtain both line emission and continuum emission images simultaneously, they have nearly the same sensitivity. Because bandwidth of both images can be precisely specified, we can minimize the systematic error due to uncertainty of the bandwidth.

ACKNOWLEDGEMENTS

This work was performed under the auspices of the U.S. Department of Energy by the University of California, Lawrence Livermore National Laboratory under contract No. W-7405-Eng-48 and the National Laser Users Facility of the University of Rochester Laboratory for Laser Energetics Grant DE-FG03-00SF22019.

REFERENCES

1. J. Lindl, Peter Amendt, Richard L. Berger et. al., Phys. Plasmas **11**, 339 (2004).
2. B. Yaakobi, R. S. Craxton, R. Epstein, and Q. Su, J. Quant. Spectrosc. Radiant. Transfer 58, 75 (1997).
3. I. Uschmann et al., Appl. Opt. 39, 5865(2000); K. Fujita et al., Rev. Sci. Instrum. 72, 744 (2001); Y. Ochi et al., Rev. Sci. Instrum. 74 1683 (2003).
4. B. Yaakobi et al., Appl. Opt. 37, 8704 (1998); J. A. Koch et al., Rev. Sci. Instrum. 70,525(1999); J. A. Koch et al., Appl Opt. 37, 1784 (1998)
5. T. R. Boehly et al., Opt. Commun. 133 495 (1997)
6. F. J. Marshall et al., Rev. Sci. Instrum. 72, 713 (2001)
7. L. A. Welser et al., Rev. Sci. Instrum.74, 1951 (2003)
8. B.L. Henke et al., Atomic Data and Nuclear Data Tables Vol. 54 (no.2), 181-342 (July 1993).
9. T. W. Barbee, Lawrence Livermore National Laboratory (personal communication).
10. W. H. Press, S. A. Teukolsky, W. T. Vetterling, B. P. Flannery, *Numerical Recipes in C*, 2nd ED. (CAMBRIDGE UNIVERSITY PRESS, CAMBTIDGE), pp. 412-420. For Fourier transform and correlation, see also pp. 496-498 and pp. 521-524.

FIGURE CAPTION

Fig. 1. Schematic of the experimental set up of the multiple monochromatic x-ray imaging. The pinhole array produce ~500 sub images onto the CID after reflection off a multi-layer Bragg mirror.

Fig. 2. Typical raw image obtained with the MMI. The obtained image has continuous spectral dispersion on its vertical axis.

Fig. 3. Fast Fourier transform of the MMI image. Low frequency region on the center is masked to show week features in middle frequency region. The node interval of grid like structure is inversely proportional to the spacing of sub images on the raw image.

Fig. 4. Quasi-monochromatic images reconstructed from the raw data shown in Fig. 2.: (a) 2.3~2.35 angstrom (below Ti K edge), (b):2.67~2.69 angstrom (with in Ti K absorption line), (c)2.75~2.80 angstrom (continuum) (d) 3.065~3.115 angstrom (continuum), (e) 3.115~3.165 angstrom (Ar-Ly-β) (f): 3.25~3.30 angstrom (continuum), (g) 3.30~3.38 angstrom (Ar-He-β), (h) 3.436~3.486 angstrom (continuum). Each image is normalized by its peak value.

FIG .1

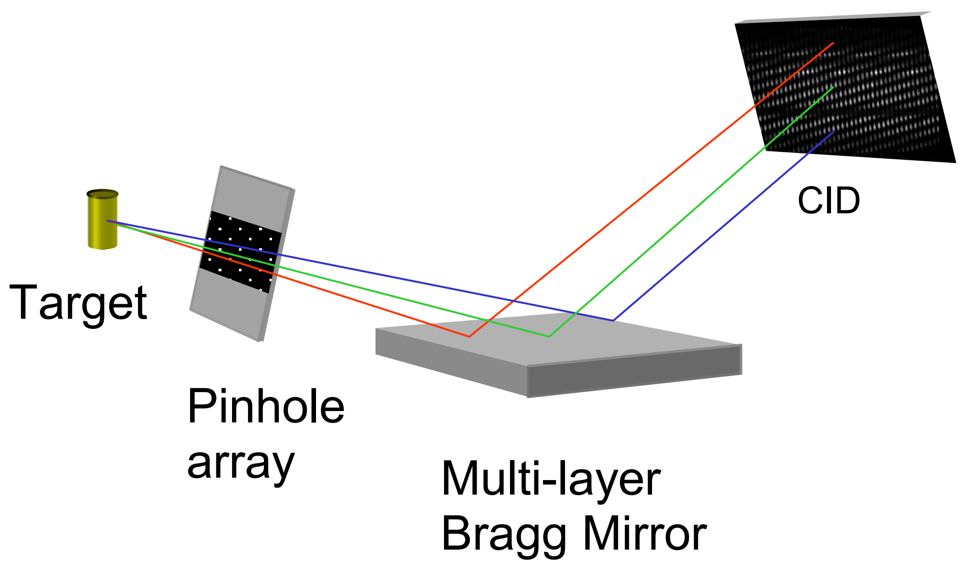

FIG 1. N. IZUMI et al., submitted to Review of Scientific Instruments

FIG. 2

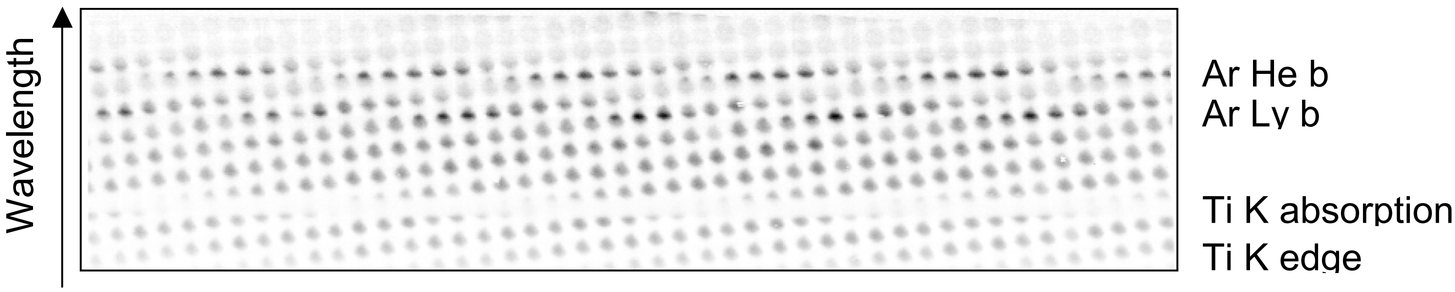

FIG 2. N. IZUMI et al., submitted to Review of Scientific Instruments

Fig. 3

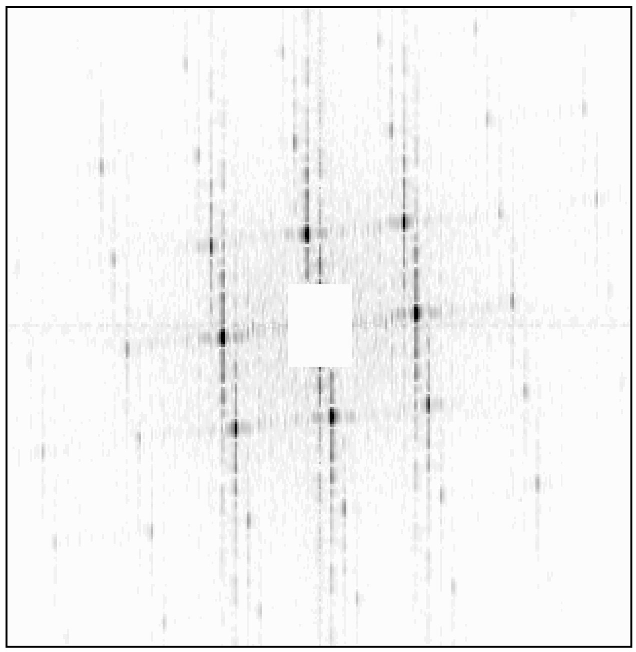

FIG 3. N. IZUMI et al., submitted to Review of Scientific Instruments

FIG. 4

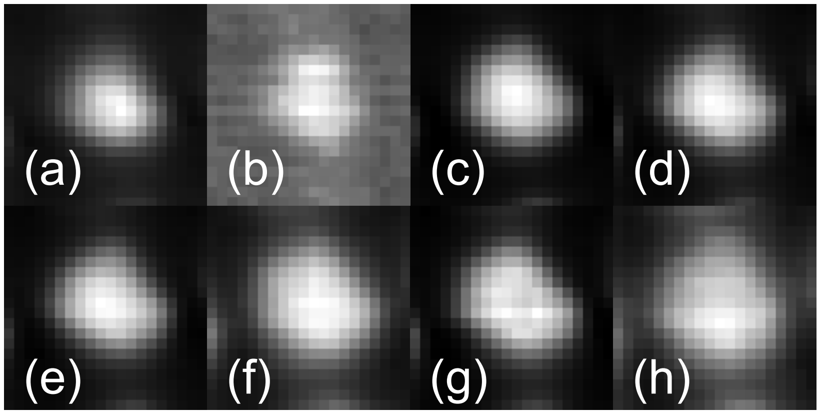

FIG 4. N. IZUMI et al., Submitted to Review of Scientific Instruments